PERGAMON

Vision Research 42 (2002) 565–575

Vision Research

www.elsevier.com/locate/visres

# Comparison of color and luminance vision on a global shape discrimination task ☆

Kathy T. Mullen *, William H.A. Beaudot

*McGill Vision Research, Department of Ophthalmology, McGill University, 687 Pine Avenue West, H4-14, Montreal, Que., Canada H3A 1A1*

Received 8 June 2001; received in revised form 1 October 2001

**Abstract**

We compared the performances of the blue–yellow, red–green and luminance systems on a shape discrimination task. Stimuli were radial frequency patterns (radially modulated fourth derivative of a Gaussian) with a peak spatial frequency of 0.75 cpd. Stimuli isolated the chromatic (red–green and blue–yellow) and achromatic post-receptoral mechanisms. We showed that in all cases performance, measured as a radial modulation threshold for discrimination between a circular and non-circular stimulus, improves with contrast. Performance was compared across radial frequencies with contrast matched in multiples of stimulus detection threshold. We find that blue–yellow color system performs the worse on this shape discrimination task, followed by the red–green, with the achromatic system performing best. The average difference is a factor of 2 between achromatic and blue–yellow performance, and a factor of 1.7 between red–green and achromatic. Despite these performance losses, chromatic shape discrimination can still reach hyperacuity performance levels. In a secondary experiment we contrast modulate the radial contour to eliminate either the ''corners'' or ''sides'' of an RF4 (square) pattern. We find that for the achromatic system, the sides are more important for the task than the corners. However, for the chromatic system, removal of sides or corners produces similar performance deficits. We conclude that color vision has a selective although relatively mild deficit for two-dimensional form perception. © 2002 Elsevier Science Ltd. All rights reserved.

*Keywords:* Shape discrimination; Color vision; Red–green; Blue–yellow; Isoluminance; Hyperacuity

## 1. Introduction

Many of the early demonstrations of the effects of isoluminance on form perception suggested that there was a fundamental impoverishment of spatial processing by color vision. The first reports of isoluminant borders described them as 'shimmery' or 'jazzy' in appearance (Gregory, 1977; Liebmann, 1927), and they are less perceptually distinct (Tansley & Boynton, 1978). Later demonstrations have shown that depth from perspective, spatial organization, and figure ground segregation can all be diminished under red–green and blue–yellow isoluminant conditions (Cavanagh, 1991; Cavanagh, Adelson, & Heard, 1992; Livingstone & Hubel, 1987, 1988). On the other hand, apart from an overall difference in the shape of the contrast sensitivity functions and in visual acuity (Kelly, 1983; Mullen, 1985; Sekiguchi, Williams, & Brainard, 1993), the early stages of form processing by color and luminance vision appear to operate in a very similar manner. Specifically, color vision, like luminance vision, appears to use an initial stage of spatial bandpass filtering. Psychophysical studies using noise masking and adaptation indicate that color vision uses arrays of bandpass filters with very similar bandwidths to those found for luminance vision (Bradley, Switkes, & DeValois, 1988; Losada & Mullen, 1995; Mullen & Losada, 1999; Switkes, Bradley, & De Valois, 1988). Furthermore, at a secondary stage of processing, in which information is integrated across space to extract rudimentary contours, color vision also performs remarkably well. This stage has been compared in color and luminance vision using a stimulus composed of arrays of Gabor elements that are linked by orientation to form a contour; color and luminance vision perform very similarly on this task (McIlhagga &

☆ This work was initially reported to the 2001 Meeting of the Association for Research in Vision and Ophthalmology, Fort Lauderdale, FL, USA (IOVS 42/4).

* Corresponding author. Tel.: +1-514-843-1231x34757; fax: +1-514-843-1691.

*E-mail address:* kathy.mullen@mcgill.ca (K.T. Mullen).

0042-6989/02/$ - see front matter © 2002 Elsevier Science Ltd. All rights reserved.
PII: S0042-6989(01)00305-4

Mullen, 1996; Mullen, Beaudot, & McIlhagga, 2000). In addition, no loss of vernier acuity has been reported for color vision, providing stimulus visibility in the relevant spatial passband is controlled (Kooi, De Valois, & Switkes, 1991; Krauskopf & Farell, 1991). What has been explored less systematically however, is the role of color beyond these stages, when local spatial information and contours are linked into definable and recognizable shapes. Thus it is likely that any deficiency of form perception in color vision is specific and confined to the higher stages, such as the analysis of shapes and the extraction of three-dimensional form.

The requirements of shape processing have been of considerable recent interest in psychophysical research. It is clear that a key aspect of simple shape processing is the binding of distributed local features into an overall form. It is generally recognized that this involves a non-linear stage of processing, based on the grouping of local information over relatively large stimulus areas to provide a 'global' representation of a shape (e.g. Wilson, 1999; Wilson & Wilkinson, 1997; Wilson, Wilkinson, & Assad, 1997; Wilkinson, Wilson, & Habak, 1998), a requirement also common to texture perception. Such a task is likely to use the prestriate cortical areas suited to the linking of distributed local information.

It is widely accepted that form processing is primarily undertaken within the ventral visual pathway, which carries information from the early stages of cortical filtering (V1, V2) to the complex object and face processing areas of the inferior temporal cortex (Desimone & Schein, 1987; Desimone, Schein, Moran, & Ungerleider, 1985; Gross, 1992). The two adjacent prestriate areas V4 and TEO lie within this pathway, and so are likely to have a key role in form perception. In particular area V4 has been extensively investigated and results give strong support to a role in shape processing. Lesions of area V4 in primates have an impact on shape discrimination (Merigan, 1996, 2000; Merigan & Pham, 1998; Schiller, 1995). Additionally, single cell recordings in primates point to a key role of area V4 in the determination of higher order structure and form analysis (Gallant, Braun, & Van Essen, 1993, 1996). The visual attribute of color is also thought to be almost exclusively analysed within the ventral cortical stream, and in particular area V4 contains a high proportion of color sensitive neurons (e.g. Zeki, 1983). Thus the coincidence of color and form processing within the ventral visual stream raises the question we address in this study, of the extent to which color vision can support shape discrimination.

In this study we investigate the performance of the two chromatic mechanisms (red–green and blue–yellow) on a shape discrimination task. The stimuli we use are radial frequency patterns, a novel stimulus set devised by Wilson and Wilkinson (1997) based on the deformation of a circle. These stimuli have been used to investigate form processing in luminance vision (Hess, Wang, & Dakin, 1999; Wilkinson et al., 1998; Wilson & Wilkinson, 1997). We use these stimuli for two reasons. First, there is evidence from luminance vision, examined more fully in Section 4, that their shape is detected using a global mechanism, in which contour information is pooled across the different parts of the object. Second, these radial frequency stimuli are non-cartesian stimuli, which have been shown to activate neurons in area V4 (Gallant et al., 1993, 1996), and are also effective stimuli for the activation of the human equivalent of area V4 (Wilkinson et al., 2000). These stimuli are thus well suited to the psychophysical investigation of tasks that are mediated by the human analogues of primate areas V4 and TEO.

## 2. Methods

### 2.1. Stimuli

The stimuli were chromatic (red–green and blue–yellow) and achromatic radially modulated D4s (fourth derivative of a Gaussian) (Wilson & Wilkinson, 1997; Wilkinson et al., 1998; Hess et al., 1999), with peak spatial frequencies of 0.75 cpd, whose contrasts were equated in multiples of detection threshold (Fig. 1). Note that in a control experiment we ascertained that detection threshold is not dependent on the radial frequency of the pattern, so the same scaling of contrast by detection threshold can be applied to all radial frequencies. We used a stimulus with relatively low peak spatial frequency in order to minimize the effects of chromatic aberrations (Bradley, Zang, & Thibos, 1992). The subject's task was to discriminate between a circular (unmodulated) and non-circular (radially modulated) stimulus. These radial frequency patterns are band-limited in spatial frequency domain, and defined by the equations:

$$\mathrm{RF}(r) = L_{\mathrm{m}}\left[1 + c(1 - 4r^2 + 4r^4/3)\mathrm{e}^{-r^2}\right] \tag{1}$$

$$r(x,y) = \frac{\sqrt{x^2+y^2} - R(x,y)}{\sigma} \tag{2}$$

$$R(x,y) = R_{\mathrm{m}}\{1 + A\sin[f_r \arctan(y/x) + \theta]\} \tag{3}$$

$$\sigma = \frac{\sqrt{2}}{\pi\omega_{\mathrm{p}}} \tag{4}$$

where $\sigma$ is the space constant of RF($r$) in degrees, $\omega_{\mathrm{p}}$ is the D4 peak spatial frequency (0.75 cpd). $R(x,y)$ is the sinusoidal radial modulation of D4s, where $R_{\mathrm{m}}$ is the mean radius (2.4°), $f_r$ is the radial frequency, $A$ is the amplitude of the radial modulation, and $\theta$ is the phase of the modulation (randomly chosen in each trial of the experiments). $L_{\mathrm{m}}$ and $c$ are the mean luminance and contrast, respectively. Circular radial frequency patterns

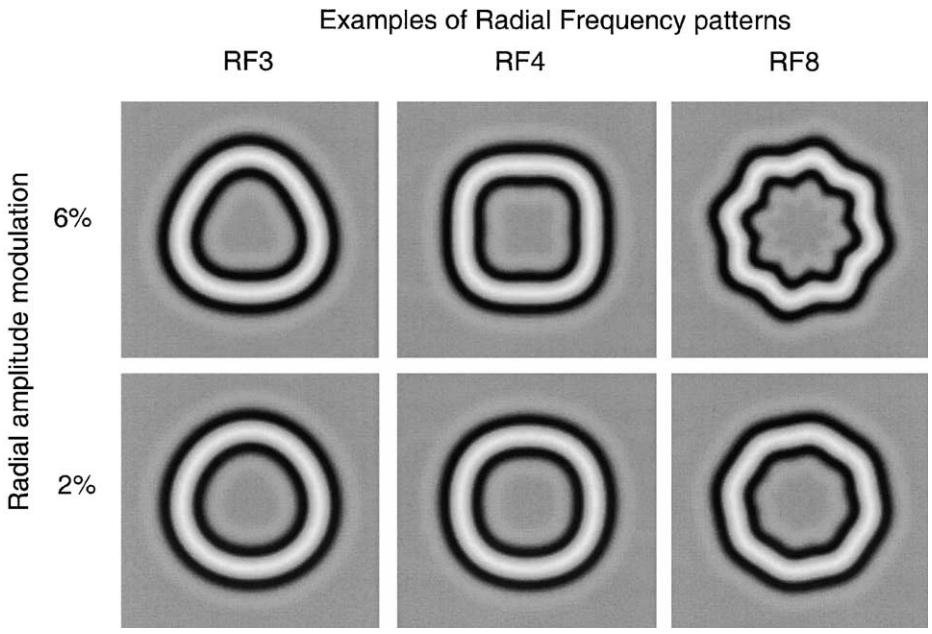


Fig. 1. Six examples of radial frequency patterns. Three radial frequencies (3, 4, and 8 cycles/circumference) and two radial modulations (6% and 2%) are shown. Increasing the radial modulation makes the shape more pronounced. Spatial frequency is 0.75 cpd and the radius is 2.4°.

have no radial modulation ($A = 0$, and thus $R$ is constant).

We also used a radially contrast-modulated version of the radial frequency pattern, defined by the equations:

$$\mathrm{RF}_C(r) = L_\mathrm{m}\{1 + c[1 - 4r^2 + 4r^4/3]\mathrm{e}^{-r^2}[1 - C(r)]\} \quad (5)$$

$$C(x,y) = C_\mathrm{m}\{1 + \sin[f_c \arctan(y/x) + \theta_c + \theta]\} \quad (6)$$

where $C(x,y)$ is the sinusoidal radial contrast modulation of D4s, $f_c$ is the radial frequency of the contrast modulation (the same as $f_r$ in our experiments), $C_\mathrm{m}$ is the factor of contrast attenuation (0.5) and $\theta_c$ is the phase of the contrast modulation (0° for sides only or 180° for corners only). Examples of these stimuli are in Fig. 5.

### 2.2. Chromatic representation of the stimuli

The chromaticity of the stimuli was defined using a three-dimensional cone contrast space in which each axis represents the quantal catch of the L, M, and S cone types normalized with respect to the white background. Stimulus chromaticity and contrast is given by a vector direction and magnitude, respectively, within the cone contrast space. In all experiments only the three cardinal stimuli were used, selected to isolate each of the three different post-receptoral mechanisms. A cardinal direction for a given mechanism is the unique direction orthogonal to the vector directions of the other two mechanisms. Previous studies have estimated the red–green, blue–yellow, and luminance mechanism directions to be approximately; L−M, S−0.5(L + M) and 3L + M (Cole, Hine, & McIlhagga, 1993; Sankeralli & Mullen, 1996). From these the cardinal direction for each mechanism is calculated (i.e. the direction in color space that lies orthogonal to two of the three mechanisms). The luminance and blue–yellow cardinal directions are L+M+S (the achromatic direction) and S, respectively. The wide intersubject variability found for the luminance mechanism affects the specification of the red–green cardinal direction. The red–green isoluminant direction was determined for each subject individually using a minimum motion technique for a patch of grating (0.75 cpd, 3.6 deg$^2$) viewed binocularly and foveally, and having the same mean luminance and chromaticity as the Gabor stimuli used in the experiments. Since the red–green isoluminant direction was specified within the L, M cone contrast plane, it was not orthogonal to the blue–yellow mechanism. Any resulting cross-stimulation of the blue–yellow mechanism would be small, however, and given the very low cone contrast sensitivity of the blue–yellow mechanism relative to the red–green (Sankeralli & Mullen, 1996) is highly unlike to influence the results. Maximum cone contrast for chromatic stimuli was limited by the display and varied across subjects according to their red–green isoluminant axis.

### 2.3. Apparatus and calibrations

Stimuli were displayed on a Sony Trinitron monitor (GDM-F500R) driven by a VSG 2/4 graphics board (Cambridge Research Systems) with 15 bits contrast resolution, housed in a Pentium PC computer. The frame rate of the display was 76 Hz. The spectral

emissions of the red, green and blue guns of the monitor were calibrated using a PhotoResearch PR-650-PC SpectraScan. The monitor was gamma corrected in software with lookup tables using luminance measurements obtained from an OptiCAL gamma correction system interface with the VSG display calibration software (Cambridge Research Systems). The Smith and Pokorny fundamentals were used for the spectral absorption of the L, M, and S cones. From these data a linear transform was calculated to specify the phosphor contrasts required for given cone contrasts (Cole & Hine, 1992). The monitor was viewed in a blacked out room. The mean luminance of the display was 60 cd/m$^2$. The stimuli were viewed at 60 cm, and subtended an area of 254 × 254 pixels (9 × 9°). Stimuli were generated on-line, and a new stimulus was generated for each presentation.

### 2.4. Protocol

For each post-receptoral mechanism we measured contrast thresholds for the detection of a circular radial frequency (RF) pattern using a 2AFC staircase procedure. In each trial, one interval contained a circular stimulus and the other contained a blank stimulus with the same average luminance. Subjects were asked to indicate which interval had the circular stimulus. In a different 2AFC staircase procedure we measured shape discrimination threshold. The radial modulation amplitude threshold for discriminating between a circular and non-circular radial frequency pattern was determined at various contrasts (expressed as multiple of contrast threshold) and radial frequencies ($f_r = 2$–32 cycles/circumference). In each trial, one interval contained a circular stimulus and the other contained a non-circular stimulus. Subjects were asked to indicate which interval had the non-circular stimulus. In both 2AFC staircase procedures, contrast or radial modulation amplitude was reduced after two correct responses, and increased after one wrong response. The change was 50% before the first reversal, and 25% after the first reversal. Each session was terminated after six reversals, and the detection threshold was computed from the mean of the last five reversals.

In both experiments, the exact location of the stimulus presented at the display centre was varied randomly from trial to trial by adding a positional jitter corresponding to 20% of the stimulus radius (±0–0.48°). The duration of each stimulus was 1 s, and the overall contrast of each stimulus was Gaussian enveloped with a sigma of 250 ms centred on the temporal window. Auditory feedback was given after each trial. A black fixation mark was presented at the beginning of each session in the centre of the display, and subjects were asked to sustain their fixation during the whole session. Practice trials were run before the experiments commenced. All experiments were done under binocular conditions.

The number of trials per session for each experiment was between 30 and 50 for each subject. Thresholds were obtained by averaging across sessions, and plotted data points show the mean of 3–6 sessions performed for each condition.

### 2.5. Observers

The observers were the two authors (KTM and WHB) and two naïve subjects (KP and AR). All have normal, or refracted to normal vision, and all have normal color vision according to the Farnsworth–Munsell 100-Hue Test.

## 3. Results

In our experiments cone contrast is expressed in multiples of detection threshold to eliminate the effects of differences in the contrast sensitivity functions of the three mechanisms, and allow stimuli to be matched in terms of suprathreshold contrast units (i.e. matched in visibility). For this scaling, detection thresholds were obtained for circular (RF = 0) red–green, blue–yellow and achromatic RF patterns using a 2AFC staircase method, with each threshold calculated as the mean of 3–5 staircase measurements. In the first experiment we investigate the effects of contrast on shape discrimination in the three mechanisms (Ach, RG, and BY). Results for shape discrimination (% threshold radial modulation) as a function of contrast for a radial frequency of 4 are shown in Fig. 2. In addition, we measured radial modulation thresholds as a function of contrast over a range of radial frequencies (4–16 cycles/circumference) for both achromatic and chromatic stimuli, with results shown in Fig. 3.

The results of these two figures show that contrast affects performance similarly for the red–green, blue–yellow and achromatic mechanism; thresholds improve continuously and proportionally with increasing contrast (note the log scales used). This contrast dependence is not dependent on the radial frequency used (Fig. 3). The second feature of the data is that thresholds for the chromatic stimuli are greater than those for achromatic ones. This difference between chromatic and achromatic stimuli is found over the whole contrast range and at all three radial frequencies tested. Third, we note that, despite the overall poorer performance with chromatic stimuli, shape discrimination still reaches hyperacuity levels at the highest contrasts. Hyperacuity levels, as defined for achromatic stimuli, occur when acuity falls below the maximum cone sampling rate of 2 per arcmin of visual angle, corresponding to a radial modulation of 0.7% on Figs. 2 and 3.

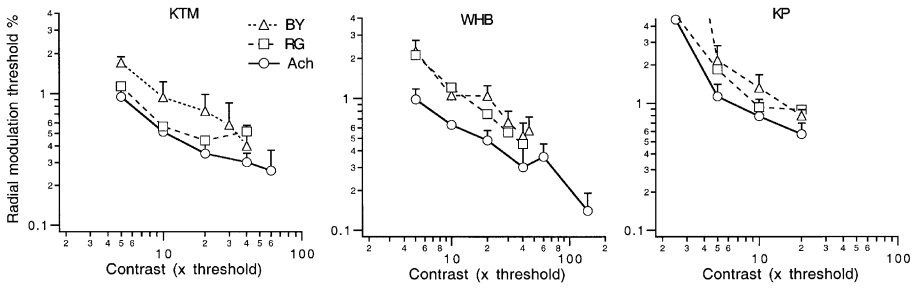


Fig. 2. Radial modulation thresholds (as a % of the radius) plotted as a function of stimulus contrast in multiples of detection threshold for the three cardinal stimuli (RG, BY, and Ach). Note that % radial modulation can be converted to units of distance by multiplying by the stimulus radius of 2.4°. Stimulus radial frequency is 4. (○) achromatic stimulus; (□) red–green stimulus; (△) blue–yellow stimulus. Results for three subjects. Error bars show +1sd.

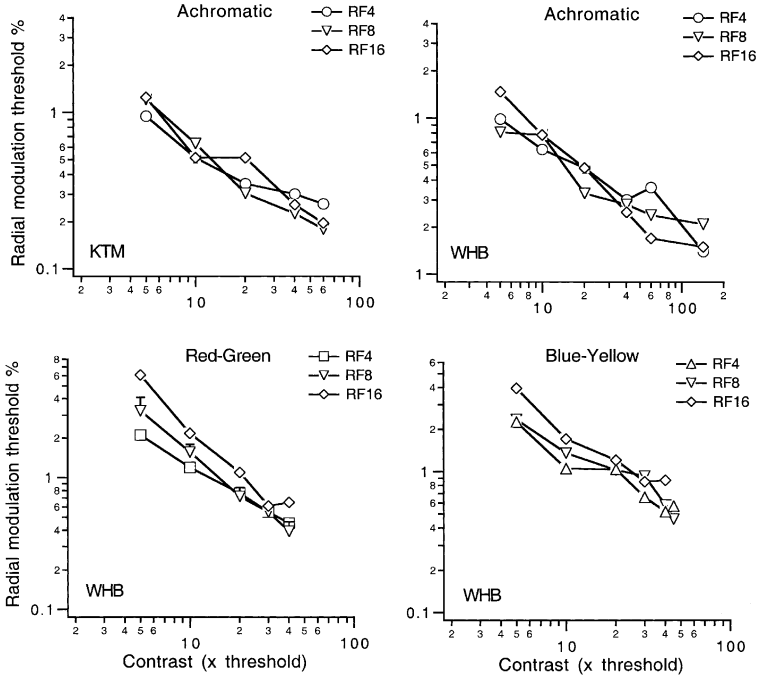


Fig. 3. Radial modulation thresholds (as a % of the radius) plotted as a function of stimulus contrast in multiples of detection threshold, for three radial frequencies. Top panels show results for achromatic stimuli in two subjects (KTM, WHB). Bottom panels show results for red–green (left) and blue–yellow (right) cardinal stimuli in subject WHB.

In Fig. 4 we investigated the effect of radial frequency on shape discrimination. The red–green, blue–yellow and achromatic stimuli were each displayed at the same constant multiple of detection threshold (5 × threshold for the two experienced subjects, 10 × threshold for the two naïve subjects). Two features of the data are evident. First, radial modulation thresholds show a shallow U-shaped dependence on radial frequency with best thresholds falling at radial frequencies of 3–6, and this effect can be seen for all mechanisms (Ach, RG, and BY) and subjects. Particularly noticeable is the rise in thresholds that occurs at higher radial frequencies. This form of result was not found in previous data using achromatic stimuli (Wilkinson et al., 1998), which showed a relatively flat dependence on radial frequency. Second, we note that the achromatic thresholds are consistently lower than the chromatic ones. In addition, thresholds for red–green stimuli are lower than for blue–yellow with the exception of WHB, who has similar red–green and blue–yellow thresholds. The average differences in log units between achromatic and BY thresholds for each subject are: 0.28 (KTM); 0.31 (WHB); 0.31 (KP); 0.40 (AR), with an overall average of 0.33 log units. The average differences in log units between the achromatic and red–green thresholds for each subject are: 0.16 (KTM); 0.26 (WHB); 0.20 (KP); 0.28 (AR), with an overall average of 0.23 log units.

In a further experiment we investigated an aspect of the mechanism of shape discrimination. We contrast modulated the radial frequency pattern (RF = 4) (see

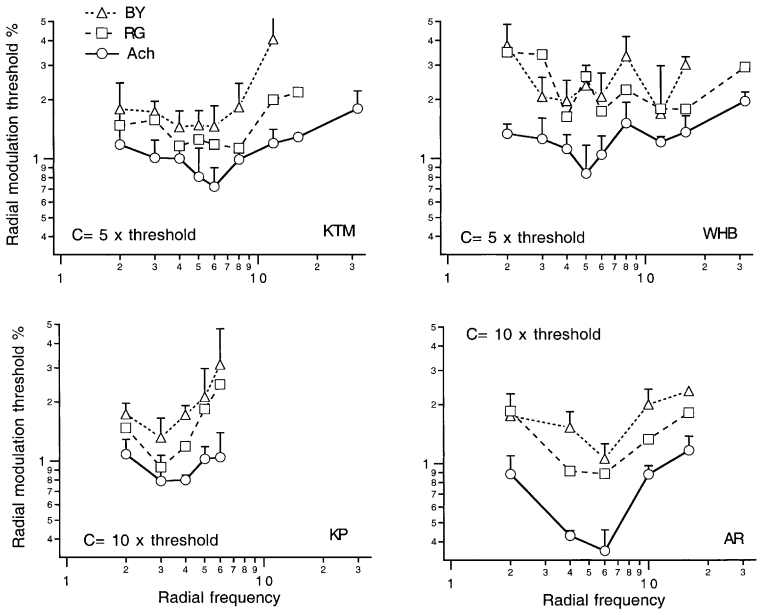


Fig. 4. Radial modulation thresholds (as a % of the radius) plotted as a function of radial frequency for the three cardinal stimuli (RG, BY, and Ach). (○) achromatic stimulus; (□) red–green stimulus; (△) blue–yellow stimulus. Results are for four subjects, shown in each panel. Contrast was fixed at 5 × detection threshold for KTM and WHB, and 10 × threshold for KP and AR. Error bars show +1sd.

Section 2) using a full contrast modulation so as to eliminate either the corners or the sides of the pattern. The appearance of the stimuli is shown in Fig. 5. Shape discrimination thresholds were then measured under these conditions for achromatic and blue–yellow patterns. Results for the achromatic pattern are shown in Fig. 6. Removing the 'corners' has a minimal impact on radial modulation thresholds compared to the full RF pattern. On the other hand, removing the 'sides' of the RF4 has a much more pronounced effect with a significant loss of performance. The average elevation of threshold in log units for the no-corners stimulus was 0.23 (KTM) and 0.16 (WHB), and the average threshold elevation for the no-sides stimulus was 0.40 (KTM) and 0.45 (WHB). These results suggest that for the achromatic pattern, the sides are more important for threshold than the corners of the pattern. Results for BY stimuli are shown in Fig. 7. In this case, the effects of removing the sides or corners of the RF patterns are similar, both causing the same intermediate loss of performance. The average elevation of threshold in log units for the no-corners stimulus was 0.20 (KTM) and 0.25 (WHB), and the average threshold elevation for the no-sides stimulus was 0.22 (KTM) and 0.31 (WHB). These results suggest that there are differences in the way the shape is analysed between the achromatic and the blue–yellow chromatic systems.

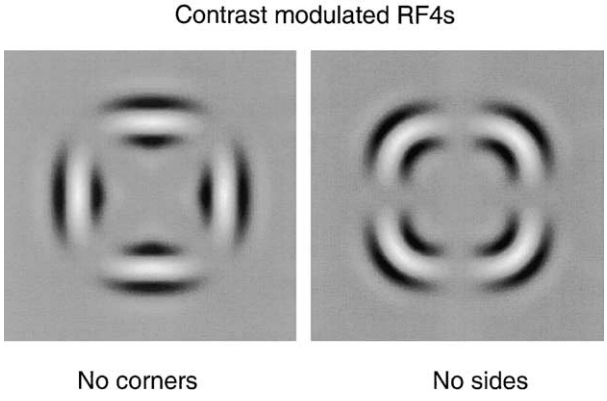


Fig. 5. Two radial frequency patterns with full sinusoidal radial contrast modulation, as defined in Eqs. (5) and (6). Two phases of contrast modulation are shown: 0° (left) which eliminates the perceptual corners of the stimulus, and 180° (right) which eliminates the perceptual sides of the stimulus. Radial frequency = 4.

## 4. Discussion

### 4.1. Shape discrimination threshold versus radial frequency

Overall, our results reveal a U-shaped dependence of shape discrimination threshold on radial frequency, with optimum performance occurring around 3–6 cycles/circumference (Fig. 4). At low radial frequencies, there is a small improvement in performance as radial frequency increase from 2, and this has also been reported in previous data (Hess et al., 1999; Wilkinson et al., 1998; Wilson & Wilkinson, 1997). Above radial frequencies of around 6–8 cycles/circumference, performance deteriorates as radial frequency increases, up to the limits of our measurements (30 cycles/circumference). It is worth

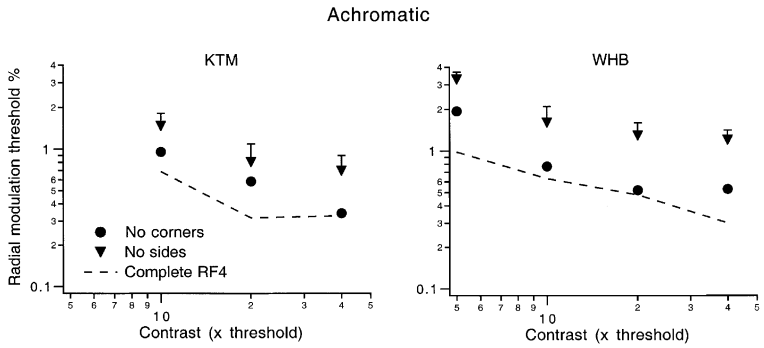


Fig. 6. Radial modulation thresholds (as a % of the radius) for radial frequency patterns with no corners (●) or no sides (▼). The dashed line shows results for the full radial frequency pattern, re-plotted from Fig. 2. Results for achromatic stimuli for two subjects (KTM and WHB). Error bars show +1sd.

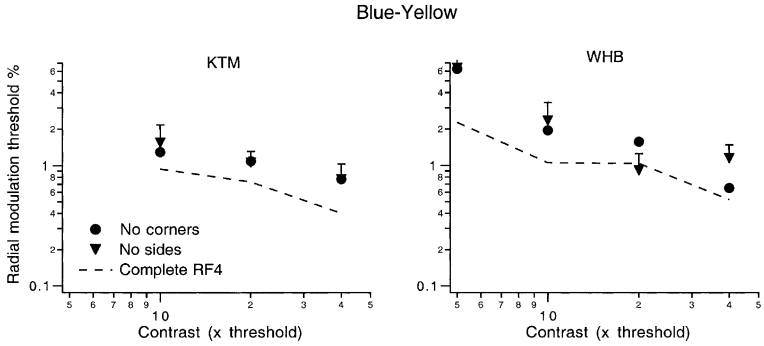


Fig. 7. Radial modulation thresholds (as a % of the radius) for radial frequency patterns with no corners (●) or no sides (▼). RF = 4. The dashed line shows results for the full radial frequency pattern, re-plotted from Fig. 2. Results for blue–yellow stimuli for two subjects (KTM and WHB). Error bars show +1sd.

noting that at these higher radial frequencies (above 8 cycles/circumference) the task changes from one of overall shape discrimination to one of identifying the modulation of the edge of a circle. Previous experiments with radial frequency stimuli have not found this high radial frequency deterioration in performance, reporting that the shape discrimination threshold remains constant as radial frequency increases (Hess et al., 1999; Wilkinson et al., 1998; Wilson & Wilkinson, 1997). Thus this high radial frequency loss in performance may depend on the choice of peak spatial frequency and/or radius of the stimuli, since previous studies have used higher peak spatial frequencies ( $\geqslant 4$ cpd) and smaller radii ( $\leqslant 1°$) than we have (0.75 cpd and 2.4° radius).

To explore the effects of spatial frequency and radius we repeated some of our measurements of shape discrimination with achromatic stimuli of a higher peak spatial frequency. We tested two new conditions: in one, the peak spatial frequency was increased from 0.75 to 3 cpd but the radius was held constant (2.4°), and in the other condition the peak spatial frequency and the radius were scaled in proportion (3 cpd, radius = 0.6°). Results are shown in Fig. 8a and compared with our original results (circles). Increasing the peak spatial frequency, but maintaining the radius (triangles) produces an overall lowering of threshold at all radial frequencies. This is contrary to previous results showing no effect of spatial frequency (Wilkinson et al., 1998). Increasing the spatial frequency, but scaling down the radius proportionally (squares), however, had little effect on the results, confirming that thresholds obey distance scaling (shape constancy) (Wilkinson et al., 1998). The overall improvement in performance associated with the increase in spatial frequency at the longer radius (triangles, 3 cpd, radius = 2.4°) is probably explained directly from the stimulus configuration. The thicker (0.75 cpd) contour is composed of inner and outer 'rings' that are quite widely separated (illustrated in Fig. 1), whereas the contour in the 3 cpd stimulus is around four times narrower. If the inner rings of the thick contour are used to judge its shape, this stimulus will effectively have a shorter radius. This is likely to account for the improved (3 cpd) thresholds in Fig. 8, as the threshold amplitude of radial modulation is inversely proportional to the radius under a range of conditions (Wilkinson et al., 1998).

Above, we suggested that the low radial frequencies require an overall shape discrimination task, whereas

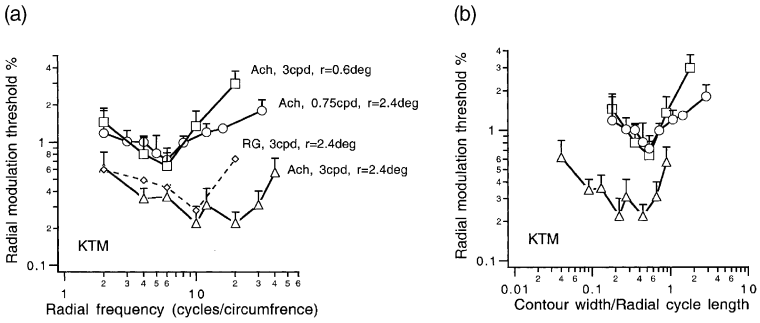


Fig. 8. (a) Radial modulation thresholds (as a % of the radius) plotted as a function of radial frequency for three different patterns each with a different peak spatial frequency or radius ($r$). Stimulus contrast is 5 × threshold. (○) Ach, 0.75 cpd, radius = 2.4° (original condition); (△) Ach, 3 cpd, radius = 2.4°; (◇) RG, 3 cpd, radius = 2.4°; (□) Ach, 3 cpd, radius = 0.6 cpd (re-scaled original stimulus). (b) Radial modulation thresholds taken from (a) with radial frequency re-plotted as the ratio of contour width per radial cycle length. Contour width is calculated as one period of the peak spatial frequency for each condition, and radial cycle length is calculated as the period of the radial frequency in circumference length. The ratio at which thresholds begin to rise at the high radial frequency end of the plot is around 0.5, or 2 contour widths per radial cycle.

higher ones are an edge-based discrimination, and hence these two parts of the function may need to be considered separately. To demonstrate this we have plotted our results in a different form, replacing radial frequency with a measure that takes into account the peak spatial frequency used in the contour, and its radial frequency. Specifically, we calculate the width of the contour in degrees (defined as one period of the peak spatial frequency) and the period of the radial modulation in degrees (reciprocal of radial frequency in units of circumference length), and express them as a ratio. Fig. 8b shows radial modulation threshold as a function of this contour width/modulation length ratio. Note that the ratio at which thresholds start to rise under all three spatial conditions are aligned, at around 0.5. In other words, approximately 2 contour widths are required to represent a radial cycle with no loss of performance, and the thinner the contour, the higher the radial frequency that can be detected without loss of performance. This limit may arise in the stimulus or be neural. It demonstrates that the loss of performance at higher radial frequencies, and hence the U-shape of the function, is based on the spatial frequency of the contour, and is a resolution based limit.

### 4.2. The comparison of color and luminance performance

Our results have shown that color performs worse than luminance vision on this shape discrimination task and, of the two chromatic mechanisms, blue–yellow performs worse than red–green. On average across our four subjects, thresholds are a factor of 2 (0.33 log units) higher for blue–yellow compared to achromatic stimuli, and a factor 1.7 higher for red–green compared to achromatic stimuli. While these differences are not large, they are constant over a wide range of radial frequencies, and over the full range of suprathreshold contrasts. It is important to note that these differences in performance between the red–green, blue–yellow or achromatic mechanisms are not the result of the differences in their respective contrast sensitivity functions, since all stimuli are narrow band in spatial frequency and have been equated in terms of their detection thresholds for each condition.

Despite these overall differences, we noted in the results that chromatic shape discrimination reaches hyperacuity levels at the highest contrasts (Figs. 2 and 3). This supports reports of chromatic vernier alignment and Gabor alignment tasks, which show that red–green color vision can perform at the hyperacuity level of resolution (Morgan & Aiba, 1985; Kooi et al., 1991; Krauskopf & Farell, 1991). Because we noted an improvement in performance for our achromatic stimuli when the peak spatial frequency was increased from 0.75 to 3 cpd (Fig. 8a) we also repeated these measures of shape discrimination for red–green stimuli at 3 cpd (small diamonds in Fig. 8a). These results confirm that color vision can reach levels of performance in the hyperacuity range. That shape discrimination is a hyperacuity task is not surprising in view of the previous literature on shape and curvature analysis (e.g. Watt & Andrews, 1982; Wilson et al., 1998). Instead, these results highlight the relatively robust and highly sensitive performance of color vision on these tasks.

The question remains as to why shape discrimination based on color falls below that found for achromatic stimuli. One possible explanation arises from differences in the encoding of orientation in the chromatic and luminance systems. Models aiming to account for global shape discrimination (so-called 'filter–rectify–filter' models) use both first and second stage filters that are orientationally selective (Wilson, 1999; Wilson & Wilkinson, 1997; Wilson et al., 1997). Arrays of second stage filters sampling different orientations perform a global concentric orientation pooling to determine its

shape. Thus both the bandwidths and the number of the orientation selective sub-units are potentially limiting in the shape discrimination task. Psychophysical results show that when differences in contrast sensitivity are taken into account and stimuli at equivalent spatial frequencies are used, orientation discrimination is poorer for chromatic compared to achromatic visual channels (McIlhagga & Mullen, 1996; Mullen et al., 2000; Reisbeck & Gegenfurtner, 1998; Webster, De Valois, & Switkes, 1990; Wuerger & Morgan, 1999). Mullen et al. (2000) also report that, for their spatially confined Gabor stimuli, the chromatic deficit is greater for the blue–yellow mechanism that the red–green, however this effect is not found with the larger grating stimuli used by Webster et al. (1990). If orientation bandwidth limits the global shape discrimination task, we might expect color vision to perform more poorly than luminance vision. As yet, however, insufficient information on orientation bandwidths is available to make quantitative predictions for global shape discrimination deficits in color vision.

Our results also suggest that the mechanism of shape analysis may differ between the color and luminance systems. We find that the elimination of the sides of an achromatic RF4 (square) pattern more severely impairs shape discrimination thresholds than the elimination of the corners, which has almost no effect. This is similar to the conclusion made by Hess et al. (1999), who removed stimulus corners or sides by noise masking. Surprisingly, this experiment repeated on blue–yellow stimuli has different results, showing that the removal of either sides or corners has a similar impact on shape discrimination. It is possible that the poorer orientation discrimination of the blue–yellow mechanism makes it hard to discriminate between the sides and corners at near threshold amplitude modulations, removing the effective advantage of the global pooling of the sides afforded to the achromatic mechanism.

### 4.3. A global versus local task?

This question asks whether the discrimination of the circular and non-circular stimuli can be made on the basis of a comparison of localized changes in orientation or curvature between the two stimuli, or whether the task is dependant on the linking of the contour information distributed across the shape. Various lines of evidence have been advanced to argue for a global shape discrimination of achromatic RF stimuli. In their original paper, Wilkinson et al. (1998) argued that local curvature could not account for discrimination because (1) RF shape discrimination thresholds are better than those obtained from simple curvature discriminations, and (2) the form of the threshold versus radial frequency function is not that predicted from the use of curvature as a threshold cue. This latter point was also used to dismiss the use of local orientation judgements. In addition, Hess et al. (1999) have shown that performance is better for an intact RF pattern than for a random rearrangement of its component parts, supporting a global shape analysis that uses all the stimulus parts rather than the use of local stimulus differences. However, so far, these arguments have only been tested on achromatic stimuli, and we cannot assume they will apply to color vision. In particular, since chromatic shape discrimination is worse than achromatic, color vision may not be taking advantage of the improved performance afford by global shape analysis, and may be relying on local cues instead. This explanation does not exclude the first possibility raised above that the task is limited by impoverished orientation information at the local level. The relevance of these two explanations can be tested psychophysically in future experiments.

### 4.4. Physiological implications

Although it is maintained over all contrasts, the difference in performance between shape discrimination for color and luminance vision is not large and certainly does not warrant color vision being considered deficient in form perception. Within the context of the present understanding of chromatic processing in striate and prestriate cortex, the relative robustness of color vision for global form perception is not surprising. Areas V1 and V2 contain many color sensitive orientationally selective neurons (Kiper, Fenstemaker, & Gegenfurtner, 1997; Johnson, Hawkin, & Shapley, 2001; Leventhal, Thompson, Liu, Zhou, & Ault, 1995) suggesting the physiological basis for a chromatic form analysis is intact at this stage. Furthermore, while V4 contains a high proportion of color sensitive neurons, it is not exclusively a 'color area' but instead appears to play an important role in shape perception (Gallant et al., 1993, 1996; Merigan, 1996, 2000; Merigan & Pham, 1998; Schiller, 1995; Schiller & Lee, 1991). Drawing on the observations that there are very low numbers of cells exclusively sensitive to color in the primate visual cortex, Lennie (1998) has argued it is fruitless to search for an exclusive or modular color pathway in the visual cortex. Our results support this view, since they suggest that form perception can be supported by either chromatic or an achromatic information, as might be expected from neurons or pathways selective for multidimensional stimulus attributes.

## Acknowledgements

This study was funded by a CIHR grant to K.T. Mullen (MOP-10819). The authors thank Anik Rawji and Kamilla Premji for help in collecting data.

## References


Bradley, A., Switkes, E., & DeValois, K. K. (1988). Orientation and spatial frequency selectivity of adaptation to color and luminance gratings. *Vision Research*, *28*, 841–856.

Bradley, A., Zang, L., & Thibos, L. N. (1992). Failures of isoluminance caused by ocular chromatic aberration. *Applied Optics*, *31*, 3657–3667.

Cavanagh, P. (1991). Vision at equiluminance. In: J. Cronly-Dillon (Series Ed.) & J. J. Kulikowski, V. Walsh & I. J. Murray (Vol. Eds.), *Vision and Visual Dysfunction:* Vol. 5. *The Limits of Vision* (pp. 234–250). Macmillan Press: New York.

Cavanagh, P., Adelson, E. H., & Heard, P. (1992). Vision with equiluminant colour contrast: 2. A large-scale technique and observations. *Perception*, *21*, 219–226.

Cole, G. R., & Hine, T. (1992). Computation of cone contrasts for color vision research. *Behavior Research Methods Instruments and Computers*, *24*, 22–27.

Cole, G. R., Hine, T., & McIlhagga, W. (1993). Detection mechanisms in L-, M-, and S-cone contrast space. *Journal of the Optical Society of America A*, *10*, 38–51.

Desimone, R., & Schein, S. J. (1987). Visual properties of neurons in area V4 of the macaque: sensitivity to stimulus form. *Journal of Neurophysiology*, *57*, 835–868.

Desimone, R., Schein, S. J., Moran, J., & Ungerleider, L. C. (1985). Contour, color, and shape analysis beyond the striate cortex. *Vision Research*, *25*, 441–452.

Gallant, J. L., Braun, J., & Van Essen, D. C. (1993). Selectivity for polar, hyperbolic, and Cartesian grating in macaque visual cortex. *Science*, *259*, 100–103.

Gallant, J. L., Conner, C. E., Rakshit, S., Lewis, J. W., & Van Essen, D. C. (1996). Neural responses to polar, hyperbolic, and Cartesian gratings in area V4 of the macaque monkey. *Journal of Neurophysiology*, *76*, 2718–2739.

Gregory, R. L. (1977). Vision with isoluminant colour contrast: 1. A projection technique and observations. *Perception*, *6*, 113–119.

Gross, C. G. (1992). Representation of visual stimuli in inferior temporal cortex. *Philosophical Transactions of the Royal Society of London*, *335*, 3–10.

Hess, R. F., Wang, Z.-Y., & Dakin, S. C. (1999). Are judgements of circularity local or global? *Vision Research*, *39*, 4354–4360.

Johnson, E. N., Hawkin, M. J., & Shapley, R. (2001). The spatial transformation of color in the primary visual cortex of the macaque monkey. *Nature Neuroscience*, *4*, 409–415.

Kelly, D. H. (1983). Spatio-temporal variations of chromatic and achromatic contrast thresholds. *Journal of the Optical Society of America*, *73*, 742–750.

Kiper, D. C., Fenstemaker, S. B., & Gegenfurtner, K. L. (1997). Chromatic properties of neurons in macaque area V2. *Visual Neuroscience*, *14*, 1061–1072.

Kooi, F. L., De Valois, R. L., & Switkes, E. (1991). Spatial localization across channels. *Vision Research*, *31*, 1627–1631.

Krauskopf, J., & Farell, B. (1991). Vernier acuity: effects of chromatic content blur and contrast. *Vision Research*, *31*, 735–749.

Lennie, P. (1998). Single units and cortical organization. *Perception*, *27*, 889–935.

Leventhal, A. G., Thompson, K. G., Liu, D., Zhou, Y., & Ault, S. J. (1995). Concomitant sensitivity to orientation, direction, and color of cells in layers 2, 3 & 4 of monkey striate cortex. *Journal of Neuroscience*, *15*, 1808–1818.

Liebmann, S. (1927). Uber des Verhalten farbinger Formen bei Helligkeitsgleichieit von Figur und Grund. *Psychologisches Forschung*, *9*, 300–353.

Livingstone, M., & Hubel, D. (1988). Segregation of form, color, movements and depth: anatomy, physiology, and perception. *Science*, *240*, 740–749.

Livingstone, M., & Hubel, D. (1987). Psychophysical evidence for separate channels for the perception of form, color, movement and depth. *Journal of Neuroscience*, *7*, 3416–3468.

Losada, M. A., & Mullen, K. T. (1995). Color and luminance spatial tuning estimated by noise masking in the absence of off-frequency looking. *Journal of the Optical Society of America A*, *12*, 250–260.

McIlhagga, W. H., & Mullen, K. T. (1996). Contour integration with color and luminance contrast. *Vision Research*, *36*, 1265–1279.

Merigan, W. H. (1996). Basic visual capabilities and shape discrimination after lesions of extrastriate area V4 in macaques. *Visual Neuroscience*, *13*, 51–60.

Merigan, W. H. (2000). Cortical area V4 is critical for certain texture discriminations, but this effect is not dependent on attention. *Visual Neuroscience*, *17*, 949–958.

Merigan, W. H., & Pham, H. A. (1998). V4 lesions in macaques affect both single- and multiple-viewpoint shape discriminations. *Visual Neuroscience*, *15*, 359–367.

Morgan, M. J., & Aiba, T. S. (1985). Positional acuity with chromatic stimuli. *Vision Research*, *25*, 689–695.

Mullen, K. T. (1985). The contrast sensitivity of human colour vision to red/green and blue/yellow chromatic gratings. *Journal of Physiology*, *359*, 381–400.

Mullen, K. T., Beaudot, W. H. A., & McIlhagga, W. H. (2000). Contour integration in color vision: a common process for the blue–yellow, red–green and luminance mechanisms? *Vision Research*, *40*, 639–655.

Mullen, K. T., & Losada, M. A. (1999). The spatial tuning of color and luminance peripheral vision measured with notch filtered noise masking. *Vision Research*, *39*, 721–731.

Reisbeck, T. E., & Gegenfurtner, K. R. (1998). Effects of contrast and temporal frequency on orientation discrimination for luminance and isoluminant stimuli. *Vision Research*, *38*, 1105–1117.

Sankeralli, M. J., & Mullen, K. T. (1996). Estimation of the L-, M- and S-cone weights of the post-receptoral detection mechanisms. *Journal of the Optical Society of America A*, *13*, 906–915.

Schiller, P. H. (1995). Effects of lesions in the visual cortex area V4 on the recognition of transformed objects. *Nature*, *376*, 342–344.

Schiller, P. H., & Lee, K. (1991). The role of the primate extrastriate area V4 in vision. *Science*, *251*, 1251–1253.

Sekiguchi, N., Williams, D. R., & Brainard, D. H. (1993). Aberration-free measurements of the visibility of isoluminant gratings. *Journal of the Optical Society of America A*, *10*, 2105–2117.

Switkes, E., Bradley, A., & De Valois, K. K. (1988). Contrast dependence and mechanisms of masking interactions among chromatic and luminance gratings. *Journal of the Optical Society of America A*, *5*, 1149–1162.

Tansley, B. W., & Boynton, R. M. (1978). Chromatic border perception: the role of red- and green-sensitive cones. *Vision Research*, *18*, 683–697.

Watt, R. J., & Andrews, D. P. (1982). Contour curvature analysis: hyperacuities in the discrimination of detailed shape. *Vision Research*, *22*, 449–460.

Webster, M. A., De Valois, K. K., & Switkes, E. (1990). Orientation and spatial frequency discrimination for luminance and chromatic gratings. *Journal of the Optical Society of America A*, *7*, 1034–1049.

Wilkinson, F., James, T. W., Wilson, H. R., Gati, J. S., Menon, R. S., & Goodale, M. A. (2000). An fMRI study of the selective activation of human extrastriate form vision areas by radial and concentric gratings. *Current Biology*, *10*, 836–838.

Wilkinson, F., Wilson, H., & Habak, C. (1998). Detection and recognition of radial frequency patterns. *Vision Research*, *38*, 3555–3568.

Wilson, H. R. (1999). Non-Fourier cortical processes in texture form and motion. In: P. S. Ulinski et al. (Eds.), *Cerebral Cortex* (pp. 445–477). New York: Kluwer Academic/Plenum Publishers.

Wilson, H. R., & Wilkinson, F. (1997). Evolving concepts of spatial channels in vision: from independence to nonlinear interactions. *Perception*, *26*, 939–960.

Wilson, H. R., Wilkinson, F., & Assad, W. (1997). Concentric orientation summation in human form vision. *Vision Research*, *37*, 2325–2330.

Wuerger, S. M., & Morgan, M. J. (1999). Input of long- and middle-wavelength-sensitive cones to orientation discrimination. *Journal of the Optical Society of America A*, *16*, 436–442.

Zeki, S. (1983). The distribution of wavelength and orientation selective cells in different areas of monkey visual cortex. *Proceedings of the Royal Society of London. Series B Biological Sciences*, *217*, 449–470.